



Cite this: *Nanoscale*, 2016, **8**, 14888

## Carbon : nickel nanocomposite templates – predefined stable catalysts for diameter-controlled growth of single-walled carbon nanotubes†

Svetlana Melkhanova,<sup>a,b</sup> Miro Haluska,<sup>c</sup> René Hübner,<sup>a</sup> Tim Kunze,<sup>†,b</sup> Adrian Keller,<sup>§,a</sup> Gintautas Abrasonis,<sup>a</sup> Sibylle Gemming<sup>a,b,d</sup> and Matthias Krause<sup>\*,a</sup>

Carbon : nickel (C : Ni) nanocomposite templates (NCTs) were used as catalyst precursors for diameter-controlled growth of single-walled carbon nanotubes (SWCNTs) by chemical vapor deposition (CVD). Two NCT types of 2 nm thickness were prepared by ion beam co-sputtering without (type I) or with assisting Ar<sup>+</sup> ion irradiation (type II). NCT type I comprised Ni-rich nanoparticles (NPs) with defined diameter in an amorphous carbon matrix, while NCT type II was a homogenous C : Ni film. Based on the Raman spectra of more than 600 individual SWCNTs, the diameter distribution obtained from both types of NCT was determined. SWCNTs with a selective, monomodal diameter distribution are obtained from NCT type I. About 50% of the SWCNTs have a diameter of  $(1.36 \pm 0.10)$  nm. In contrast to NCT type I, SWCNTs with a non-selective, relatively homogeneous diameter distribution from 0.80 to 1.40 nm covering 88% of all SWCNTs are obtained from NCT type II. From both catalyst templates predominantly separated as-grown SWCNTs are obtained. They are free of solvents or surfactants, exhibit a low degree of bundling and contain negligible amounts of MWCNTs. The study demonstrates the advantage of predefined catalysts for diameter-controlled SWCNT synthesis in comparison to *in situ* formed catalysts.

Received 8th October 2015,  
Accepted 15th July 2016

DOI: 10.1039/c5nr06972f

[www.rsc.org/nanoscale](http://www.rsc.org/nanoscale)

### Introduction

Carbon nanotubes have been known for more than 20 years<sup>1</sup> and since the very first reports on their synthesis fascinating electronic properties of CNTs were predicted. It was expected that they will be used in many fields of molecular electronics, *viz.* in transistors,<sup>2–4</sup> medical devices,<sup>5,6</sup> chemical and biochemical sensors<sup>7,8</sup> *etc.* However, in currently commercialized applications CNTs are mainly used as additives to improve the mechanical, thermal, and electrical properties of bulk materials (resins, plastics, polymers).<sup>9</sup> Semiconducting SWCNTs are well suited for transistors because of their low electron scattering and small bandgap.<sup>10</sup> For “high-tech” applications, however, precisely-defined electronic properties are needed. This requires eventually one specific diameter and chiral angle of SWCNTs.<sup>11,12</sup> There are several methods of

CNTs synthesis,<sup>13–15</sup> and among them CVD is the most versatile and most easily scalable one. The structural and morphological properties of CVD-grown CNTs are affected by many process parameters,<sup>15</sup> such as the carbon precursor nature and concentration, carrier gas pressure and composition, temperature, time, catalyst nature and size, *etc.* There are many reports that catalyst particles must have a suitable size in order to be active for CNT growth and that the control of the catalyst nanoparticles before and during CVD is very important in order to control CNT yield, diameter and chirality. The most used catalysts for CNT growth are Fe,<sup>16–31</sup> Co,<sup>24,32–45</sup> Ni<sup>17,23,46–53</sup> and their bimetallic alloys.<sup>38,42,54–56</sup> The CNT synthesis on these catalysts may produce SWCNTs with narrow diameter distribution and few chiralities depending on the catalyst nanoparticle size.<sup>16,20,21,25,26,32,35,41,51,54</sup>

In almost all studies, the catalysts are prepared *in situ* by an initial annealing step of the precursor prior to CVD or by precursor injection during the CVD process. The control of catalyst size and shape depends on many process parameters in a complex manner, whose optimization often requires numerous iterations.<sup>27</sup> The process could be simplified by introducing catalyst templates with predefined NP size and shape, which exhibit sufficient stability against coalescence and grain coarsening. Carbon : nickel nanocomposite (C : Ni NC) thin films of 10 nm to 100 nm thickness have been grown in a large variety of microstructures. This was achieved by variation of

<sup>a</sup>Helmholtz-Zentrum Dresden-Rossendorf, Bautzner Landstraße 400, 01328 Dresden, Germany. E-mail: matthias.krause@hzdr.de

<sup>b</sup>Technische Universität Dresden, cfaed, 01062 Dresden, Germany

<sup>c</sup>Micro and Nanosystems, DMAVT ETH Zürich, 8092 Zürich, Switzerland

<sup>d</sup>Technische Universität Chemnitz, 09107 Chemnitz, Germany

† Electronic supplementary information (ESI) available. See DOI: 10.1039/c5nr06972f

‡ Present address: Fraunhofer-Institut für Werkstoff- und Strahltechnik, 01277 Dresden, Germany.

§ Present address: Universität Paderborn, 33098 Paderborn, Germany.



deposition temperature (RT to 500 °C) and Ni concentration (5 to 30 at% Ni) during thin film growth without and with irradiation by an assisting low-energy Ar<sup>+</sup> beam. So far, C:Ni NCs were reported with NP diameters from 1.5 nm to 17 nm, spherical and columnar shapes, and in regular or stochastic three-dimensional particle arrangements.<sup>57–59</sup> In our previous work on SWCNT growth<sup>48</sup> we reported the successful growth of individual SWCNTs with a Gaussian-like, non-selective diameter distribution of (1.6 ± 0.4) nm from 10 nm thick templates consisting of columnar Ni NPs of (4.0 ± 1.0) nm diameter before the CVD growth process.

In this work, the SWCNT diameter distributions obtained by CVD from two 2 nm thick C:Ni NC template types are compared. NCT type I comprises predefined catalyst NPs, while for NCT type II the catalyst NPs are formed *in situ* during the CVD process. This approach enables a direct comparison of the SWCNT growth from pre-defined and *in situ* formed catalyst particles. Transmission electron microscopy (TEM) and scanning electron microscopy (SEM) were applied to characterize the NCTs before and after the CVD process and to determine the size distribution of the catalyst particles. SWCNT diameter distribution and the presence of multi-walled CNTs were analysed by SEM and Raman spectroscopy. It is demonstrated that SWCNT diameters strongly depend on the NCT type applied for CVD synthesis. Using NCT type I about 50% of the SWCNTs have a diameter of (1.36 ± 0.10) nm, while SWCNTs with a relatively homogeneous diameter distribution from 0.8 nm to 1.4 nm are obtained from NCT type II. Furthermore it is shown that MWCNT formation, SWCNT bundling, and catalyst NP coarsening are successfully suppressed. Finally, the possibilities and limits of SWCNT diameter control by defining the catalyst NP size are discussed.

## Experimental

The NCT type I (C:Ni, ~15 at% Ni) was deposited at 300 °C by ion beam co-sputtering of a graphite/Ni zone target onto a Si/SiO<sub>2</sub> (~0.5 μm, thermally oxidized) substrate. Template type II (C:Ni, ~8 at% Ni) was prepared at RT by irradiating the growing C:Ni film with an oblique incidence angle (~60°) assisting Ar<sup>+</sup> beam of 130 eV ion energy. The sputter ion source (Kaufmann type, IonTech Inc., Fort Collins, USA) was operated with an Ar<sup>+</sup> ion energy of 1 keV and a beam current of 40 mA, the assisting ion source (Kaufmann type, ISQ40KF, Ion-Tech GmbH, Wüstenbrand, Germany) with Ar<sup>+</sup> energies of 50 to 130 eV and a total beam current of 9 mA. The base pressure in the deposition chamber was (1.3 ± 0.3) × 10<sup>-5</sup> Pa, the working pressure was about 10<sup>-2</sup> Pa, and the deposition time was 3 to 4 min. The given film composition was extrapolated from the Rutherford Backscattering analysis of our previous work.<sup>57–59</sup> Further deposition details are described *ibid.*

The subsequent CVD process consists of two consecutive steps: the NCT pre-treatment and the CNT growth. For this, the C:Ni templates were placed in the CVD oven (Black Magic, Aixtron) and exposed to flowing air (flow rate 200 sccm,

pressure 2 to 3 mbar) for 10 min at 550 °C. After 10 min the reactor was evacuated, the temperature was increased to 735 °C, and the samples were exposed to a mixture of C<sub>2</sub>H<sub>2</sub>/H<sub>2</sub>/Ar (5/300/300 sccm; total pressure 5.1 mbar) for ~20 min.

Cross-sectional transmission electron microscopy images of C:Ni thin films were obtained using an image Cs-corrected Titan 80–300 (FEI) microscope operated at an acceleration voltage of 300 kV. TEM specimens of the C:Ni templates before CNT growth were prepared by sawing, grinding, dimpling, and final Ar ion milling. TEM lamella preparation of the C:Ni templates after pre-treatment and CNT growth was done by *in situ* lift-out using a Zeiss Crossbeam NVision 40 system. To protect the sensitive surface, a carbon cap layer was deposited beginning with electron beam assisted and subsequently followed by Ga focused ion beam (FIB) assisted precursor decomposition. Afterwards, the TEM lamella was prepared using a 30 keV Ga FIB with adapted currents. Its transfer to a 3 post copper lift-out grid (Omniprobe) was done with a Kleindiek micromanipulator. To minimize sidewall damage, Ga ions of only 5 keV energy were used for final thinning of the TEM lamella to electron transparency. SEM of the NCTs before and after CVD growth of the CNTs was performed by detecting secondary electrons using a S-4800 microscope (Hitachi) operated at an accelerating voltage of 10 kV. Raman maps of randomly selected sample areas of 20 × 20 μm<sup>2</sup> were recorded with a step width of 1.25 μm using a micro-Raman Labram HR spectrometer, which is equipped with a holographic 1800 lines per mm grating and a liquid nitrogen cooled CCD detector (Horiba-Jobin-Yvon). The laser wavelengths of 532 nm and 632.8 nm, corresponding to photon energies of 2.33 eV and 1.96 eV, respectively, were used for excitation. The obtained Raman spectra were fitted using an in-house software routine based on a Levenberg-Marquardt least-square algorithm. SWCNT diameter distributions were calculated by using the relation  $d_{\text{SWCNT}} = 232 \text{ cm}^{-1} \text{ nm}/\nu_{\text{RBM}}$ ,<sup>60</sup> wherein  $\nu_{\text{RBM}}$  represents the Raman shift of the radial breathing mode of SWCNTs, and by sorting the obtained diameter values into diameter intervals of 0.05 nm width.

## Results

The microstructure of the original NCT type I is heterogeneous and consists of Ni-rich particles embedded in an amorphous carbon (a-C) matrix (Fig. 1). Cross-sectional TEM analysis gives a mean NP diameter of (2.0 ± 0.3) nm, which corresponds to the average NCT thickness. The NPs appear to be well-aligned with a mean NP center to center distance of (4.3 ± 0.3) nm. Lattice fringes were resolved for approximately 40% of 27 NPs analyzed in detail (Fig. 1b and c). Fast Fourier Transform (FFT) analysis gave lattice spacings grouped into (a) 0.22 nm to 0.24 nm and (b) 0.20 to 0.21 nm. In one case crossed lattice fringes with spacings of 0.21 nm and 0.15 nm enclosing an angle of 46° were observed. The latter values are in good agreement with reference data of the (006) and {116} planes of rhombohedral Ni<sub>3</sub>C (rh-Ni<sub>3</sub>C), which are 0.215 nm, 0.156 nm,



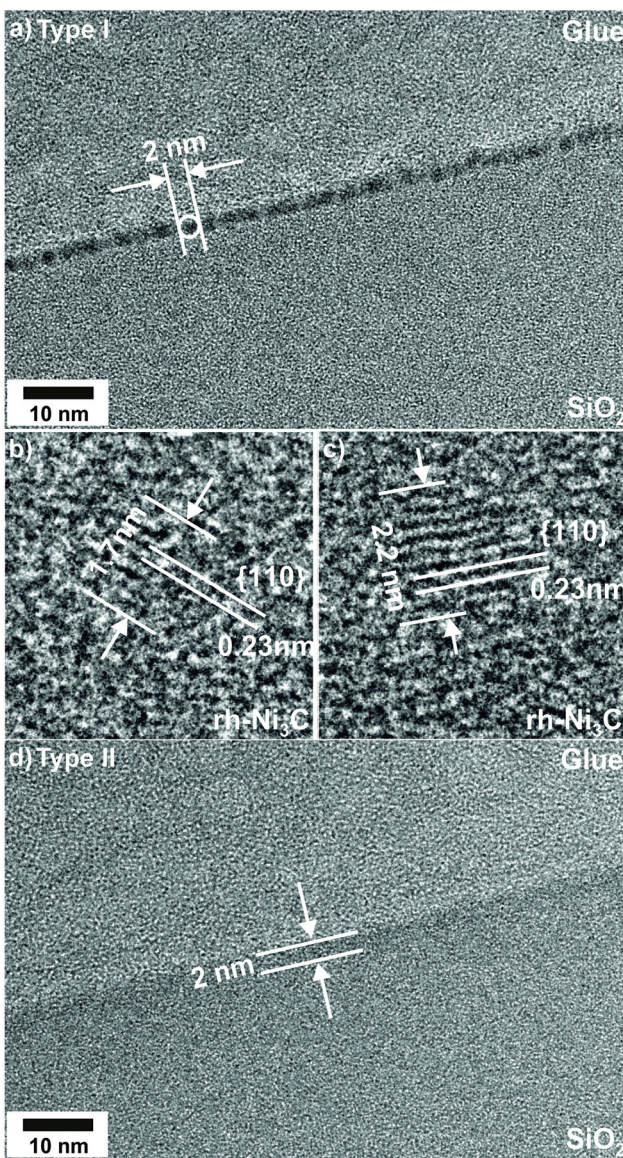


**Fig. 1** Cross-sectional TEM images of C:Ni templates before the CVD process of CNTs: (a)–(c) NCT type I; (d) NCT type II. Images (b) and (c) are enlarged views of micrograph (a) showing selected crystalline  $\text{Ni}_3\text{C}$  NPs in NCT type I.

and  $43.4^\circ$ .<sup>61</sup> Moreover, the group (a) lattice fringe spacings are indicative for rh- $\text{Ni}_3\text{C}$ , namely for its  $\{110\}$  planes.<sup>61</sup> Group (b) spacings could be assigned either to rh- $\text{Ni}_3\text{C}$  or to fcc-Ni. According to these findings, previous own work, and the literature on this material system, the initial Ni-rich phase of NCT type I is assigned to rh- $\text{Ni}_3\text{C}$ .<sup>57,62–64</sup>

The cross-sectional TEM image of NCT type II (Fig. 1d) shows the formation of a Ni-enriched layer appearing darker than the  $\text{SiO}_2$  substrate and the resin glue on top of the film, which is used for TEM specimen preparation. The layer thickness is 2 nm and hence the same as for the NCT type I. In contrast to NCT type I, no NP formation was detected for NCT type II (Fig. 1d). The homogenous microstructure of C:Ni NCT type II is attributed to the hyperthermal particle and energy flux of

the irradiating  $\text{Ar}^+$  ions. It causes ion-enhanced mixing and partial re-sputtering of Ni, which lead to a homogenous distribution of the metal in the a-C matrix.

After CVD growth of CNTs the morphology of NCT I consists of individual NPs as before the CVD process (Fig. 2).

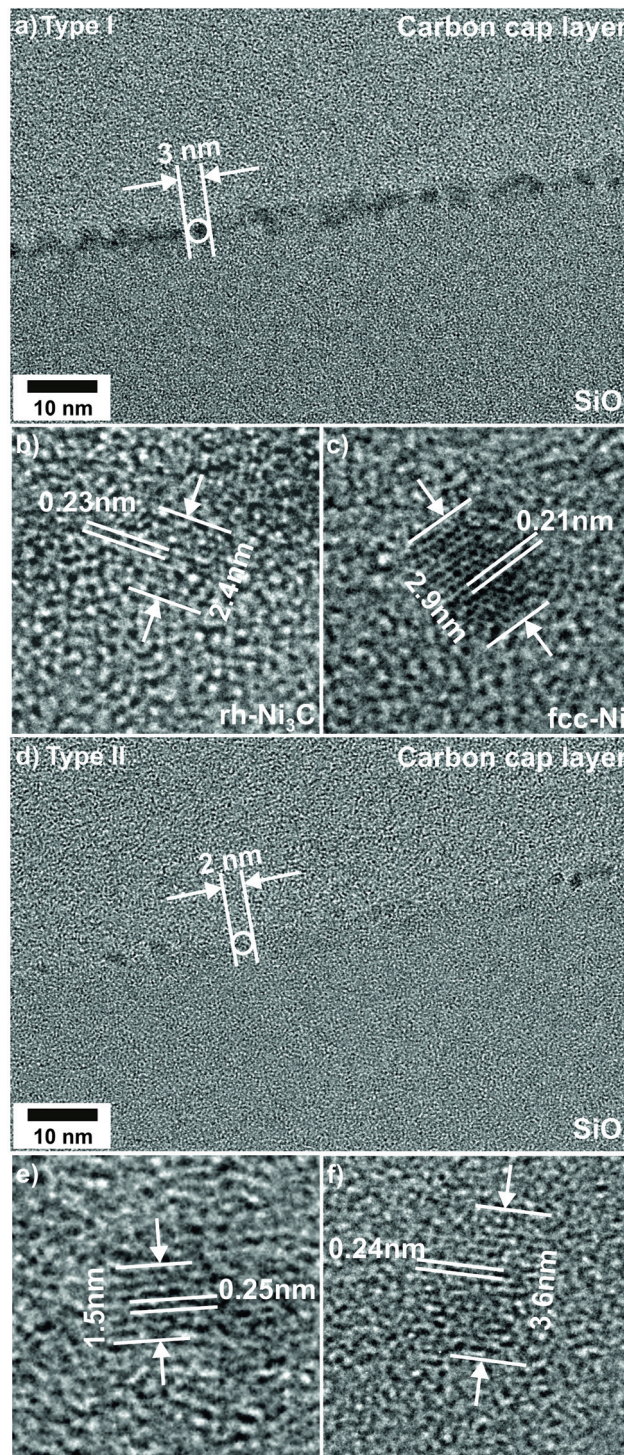


**Fig. 2** Cross-sectional TEM images of C:Ni templates after CVD growth of CNTs: (a)–(c) NCT type I; (d)–(f) NCT type II. Images (b) and (c) [(e) and (f)] show selected crystalline NPs in NCT type I [NCT type II].



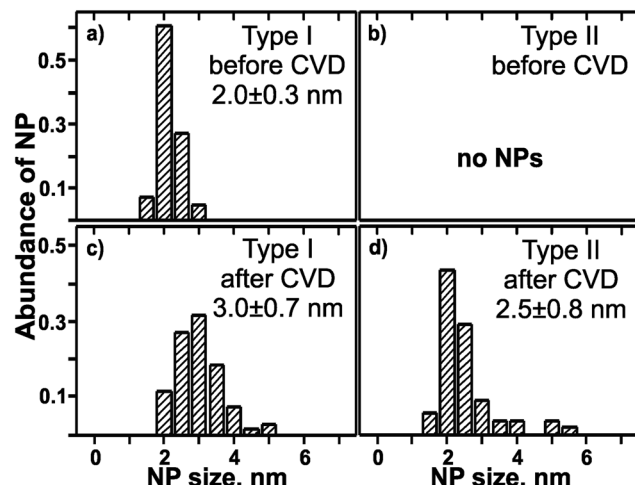


**Fig. 3** Normalized size distributions of Ni-rich NPs measured by TEM before and after the CVD process, respectively. NCT type I, (a) and (c), NCT type II, (b) and (d).

Cross-sectional TEM revealed moderate NP coarsening accompanied by broadening of the diameter distribution from initially  $(2.0 \pm 0.3)$  nm to  $(3.0 \pm 0.7)$  nm (Fig. 3). The NPs are less aligned and the NCT surface appears rougher than before the CVD process. Lattice fringes were observed for 72% out of 29 NPs studied in detail. FFT analysis revealed the coexistence of Ni-rich NPs with hcp (Fig. 2b) and fcc (Fig. 2c) lattice structure in an approximately equal ratio. The details of this analysis are provided in the ESI.† The FFT of the nanocrystal in Fig. 2b corresponds very closely to a  $[1\bar{2}1\bar{3}]$  zone axis image of hcp-Ni (for details see ESI, Fig. 1†).<sup>65</sup> It has the same Ni sub-lattice structure as rh-Ni<sub>3</sub>C. The nanocrystal displayed in Fig. 2c has fcc crystal structure. Its FFT corresponds to a  $[011]$  zone axis image of fcc-Ni (for details see ESI, Fig. 2†).<sup>65</sup> One out of 29 FFT patterns showed lattice fringes with spacings of 0.22 nm and 0.25 nm enclosing an angle of 56°. One possible assignment would be fcc-NiO, although the observed spacings were enlarged by about 4% compared to the reference.<sup>61</sup> Alternatively, this FFT pattern might be described by Ni<sub>3</sub>C  $\{110\}$  and  $\{014\}$  lattice fringes, whose spacings are 0.22 nm and 0.25 nm with an interplanar angle of 56.7°.

In summary, approximately 50% of NCT type I NPs changed their lattice structure from rh-Ni<sub>3</sub>C to fcc-Ni. For another approximately 50% the observed hcp-Ni lattice structure points to the conservation of the initial rh-Ni<sub>3</sub>C phase structure. The formation of fcc-NiO could not be verified. Finally it should be noted that TEM analysis is not suitable to provide information about the structure of the a-C matrix.

The morphology of NCT type II, where initially only a contrast enhancement with respect to SiO<sub>2</sub> substrate and resin glue could be detected, was completely changed during the CVD process. The initial homogenous and 2 nm thick Ni-enriched layer was no more detected. Instead, NCT type II is characterized by the coexistence of ranges without (major fraction) and with (minor fraction) separated NPs after the CVD

(Fig. 2d). Their average diameter is  $(2.5 \pm 0.8)$  nm (Fig. 3). The smallest resolved NP had a diameter of 1.5 nm. Two dominant lattice spacings were identified by FFT analysis, namely 0.21 nm and 0.25 nm. Their assignment to rh-Ni<sub>3</sub>C, fcc-Ni, or fcc-NiO is ambiguous as outlined in the previous sections, and supporting interplanar angles could not be determined. The NP formation from NCT type II can be considered as an example for the SWCNT growth using catalysts, which are formed *in situ* during the process of pre-treatment and CVD. The post-CVD NP diameter distribution of NCT type I is narrower than that of NCT type II. This difference can be expressed as relative deviation from the mean NP diameter values. It is 23% for NCT type I and 32% for NCT type II. Moreover, compared to NCT type II, a larger fraction of NCT type I NPs showed lattice fringes. This is a hint for a larger degree of NP crystallinity in NCT type I than in type II after the CVD growth of CNTs.

The TEM results show that the microstructure of the pre-defined NCT type I is largely preserved during the CNT growth process. Its mean NP diameter grew by about 1 nm (*ca.* 50%), and the fraction of crystalline NPs within the template increased. In contrast to that NCT type II underwent a complete re-structuring from a homogenous film into a film of NPs. The NP size distribution for NCT type II after CVD is sufficiently narrow and can be compared with the one obtained from metallic thin films. As an example, pre-annealing of a 0.22 nm-thin Ni film produced NPs with diameter of  $(4.4 \pm 0.6)$  nm.<sup>52</sup>

In contrast to the featureless appearance before nanotube growth, SEM images of the NCT samples measured after the CVD process display three types of features: (i) randomly distributed spherical spots of less than 10 nm in diameter, (ii) bent objects of about 80 nm length, and (iii) blurred objects of up to 3  $\mu$ m length (Fig. 4). These features are assigned to metallic nanoparticles, multi-walled CNTs (MWCNTs), and single-

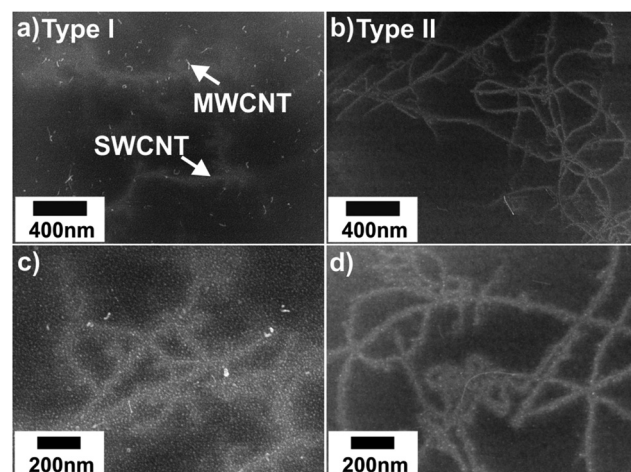


**Fig. 4** SEM images of C:Ni templates after CVD growth of CNTs: (a), (c) NCT type I; (b), (d) NCT type II. Compared to the few MWCNTs appear blurred and diffuse due to charging effects and probably also due to thermally-induced vibrations.



walled CNTs, respectively. The NP diameters are apparently larger for NCT type I than for type II. The amount of MWCNTs is generally very low. In NCT type II samples MWCNTs are virtually absent. The statistical analysis of the SEM images points to a similar efficiency of both types in catalyzing SWCNT growth with yields of  $\sim 5$  to  $7$  tubes per  $\mu\text{m}^2$ .

Raman spectroscopy enables a non-destructive and simple determination of the SWCNT diameter because of the inverse proportionality of diameter and radial breathing mode (RBM) frequency. Hence, the diameter distribution of SWCNTs in the sample can be conveniently elucidated by measuring Raman spectra with two or more excitation laser wavelengths, for example, 532 nm and 632.8 nm. This approach allows detecting SWCNTs in the diameter range from  $0.6$  nm to  $2.3$  nm. The reliability of the SWCNT diameter distribution obtained by this method was confirmed by parallel Raman and High-Resolution TEM studies in the literature.<sup>16,37</sup>

Typical Raman spectra in the range of the RBM obtained during 2D Raman mapping with two excitation wavelengths for NCT types I and II are shown in Fig. 5a and b. The vast majority of the spectra contains only one single RBM line. In total, the Raman spectra of more than 600 individual SWCNTs were analysed in this study. The RBM line widths for SWCNTs grown with both template types cover the range of  $4\text{ cm}^{-1}$  to  $8\text{ cm}^{-1}$ . They decrease with increasing RBM frequency, similar to the results reported previously in the literature.<sup>66</sup> The narrow line widths point to long lifetimes of the excited RBM modes, and indicate a high degree of structural order and a negligible contribution of defect-induced phonon decay processes. Such a behavior is consistent with the formation of individual SWCNTs with a low amount of structural defects.<sup>67</sup> In order to analyze the abundance of SWCNTs, the observed RBM frequencies were assigned to frequency intervals of  $10\text{ cm}^{-1}$  width and subsequently summed. The analysis shows

a diameter-selective SWCNT formation for NCT type I: 50% of all observed tubes have RBM frequencies from  $160\text{ cm}^{-1}$  to  $180\text{ cm}^{-1}$  (Fig. 5c). In contrast to that, a broad distribution of RBM frequencies is found for NCT type II (Fig. 5d). The corresponding diameter distributions of SWCNTs (normalized to 1) are shown in Fig. 6. The SWCNT diameter distribution depends strongly on the template type. The diameter distribution of NCT type I reveals an astonishingly high selectivity for SWCNTs of the diameter interval centered at  $(1.360 \pm 0.025)$  nm, which includes about 33% of the SWCNTs (Fig. 6a). Moreover, 51% of all synthesized SWCNTs fall into a narrow diameter range of  $1.26$  nm to  $1.46$  nm.

Applying the formula for the nanotube diameter  $d$ ,

$$d = (a_0/\pi)\sqrt{n^2 + nm + m^2},$$

with the lattice constant  $a_0 = 0.246$  nm and the chiral indices  $n$  and  $m$ , in total 9 SWCNT chiralities can be expected in the diameter range of  $(1.360 \pm 0.025)$  nm. Two of them are metallic, 7 are semiconducting. The analysis of the electronic transition energies of these 9 chiralities shows that only the  $E_{33}$  electronic transition of semiconducting SWCNTs is in resonance with the laser energy of  $2.33\text{ eV}$ .<sup>68</sup> This criterion requires that the difference between laser and electronic transition energy is  $\Delta E \leq \pm 0.10\text{ eV}$ .<sup>69</sup> The combination of these two informations reduces the chiralities preferentially observed in this study to three: (12,8), (17,1), and (16,3).

The proposed diameter selectivity is further supported by the following findings of the Raman analysis. The next thinner SWCNTs, which are expected to be in resonance with laser radiation of 532 nm, would be (13,6), (14,4) and (15,2) with diameters of  $1.32$  nm,  $1.28$  nm and  $1.26$  nm and RBM frequencies of  $175$  to  $185\text{ cm}^{-1}$ , respectively. Their abundance is only of the order of 5% (Fig. 6). At slightly larger diameters than  $(1.360 \pm 0.025)$  nm the SWCNTs (15,5), (11,10) and (14,7) with  $1.41$  nm,  $1.43$  nm and  $1.45$  nm should resonate with 532 nm laser excitation. The abundance of this fraction is about 7%. That means that the low and high limit of the SWCNT diameter distribution maximum is precisely defined for NCT type I.

It can be further concluded that semiconducting tubes with diameters of  $\sim 1.6$  nm and RBM frequencies of around

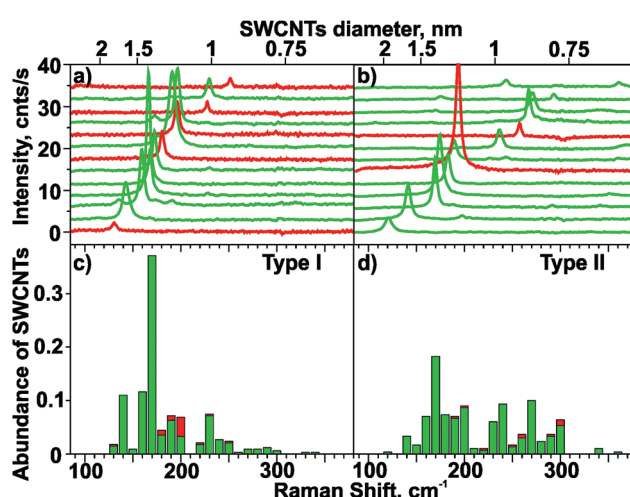


Fig. 5 Selected RBM range Raman spectra (a, b) and RBM distributions (c, d) of SWCNTs formed from C : Ni templates: (a), (c) NCT type I; (b), (d) NCT type II. The color code represents spectra measured with 532 nm (green) and 632.8 nm (red) laser excitation, respectively.

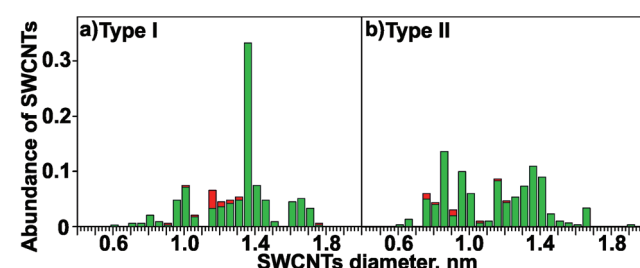


Fig. 6 Normalized diameter distributions of SWCNTs synthesized from C : Ni templates as derived from the abundance of observed RBM lines in the corresponding diameter intervals: (a) NCT type I; (b) NCT type II. The color code represents data obtained with 532 nm (green) and 632.8 nm (red) laser excitation, respectively.



140  $\text{cm}^{-1}$  contribute only to a minor extent to the observed diameter distribution (Fig. 6). Finally, for 632.8 nm laser excitation, the most abundant SWCNTs have RBM frequencies of around  $\sim 200 \text{ cm}^{-1}$  for NCT type I. They belong to metallic tubes with a diameter of 1.2 nm, whose  $M_{11}$  transition is in resonance with the laser energy of 1.96 eV. These metallic tubes cause the local maximum in the diameter distribution for 632.8 nm laser excitation, but their contribution to the overall SWCNT diameter distribution is of the order of less than 5%.

In contrast to type I, NCT type II yields a relatively uniform distribution of SWCNT diameters from 0.8 to 1.4 nm (88% of all SWCNTs). The gap of the diameter distribution at about 1.15 nm, which is also observed for NCT type I, is explained by the missing resonance of such SWCNTs with 532 nm laser radiation. For this reason the diameter distribution is not described as bimodal but as uniform. The upper limit of the SWCNT diameter distribution obtained with NCT type II is defined by the very low amount of SWCNTs with an RBM frequency of about 140  $\text{cm}^{-1}$  (<5%) corresponding to diameters of about 1.7 nm. The high overall yield of SWCNT with small diameters (40% in the 0.6–1.0 nm range) is however remarkable.

Since NCT type I is apparently a very promising pre-defined and stable catalyst for diameter-selective SWCNT growth, its morphology after pre-treatment was investigated. For this purpose the growth process was terminated after the pre-treatment step (exposing the NCTs to flowing air at 550 °C for 10 min) and the pre-treated template was analyzed using cross-sectional TEM and Raman spectroscopy (Fig. 7). The Raman

spectra of NCT type I show the typical  $\text{sp}^2$ -carbon ( $\text{sp}^2\text{-C}$ ) Raman lines, *i.e.* the D line at around 1350  $\text{cm}^{-1}$  and the G line at around 1550  $\text{cm}^{-1}$ , before and after pre-treatment (Fig. 7a). The intensity of the  $\text{sp}^2\text{-C}$  Raman lines decreased to 30% after the pre-treatment, and simultaneously the intensity of the Si-2TO lines at around 950  $\text{cm}^{-1}$  increased by approximately 40% (not shown). These observations point to a partial loss of a-C, presumably by oxidation to  $\text{CO}_2$ . Moreover, narrower line widths and G line up-shift indicate a higher degree of graphitization of the a-C matrix. Cross-sectional TEM analysis reveals a mean NP diameter of  $(2.2 \pm 0.4)$  nm, which is the same as in the virgin NCT within the experimental accuracy. In conclusion, the pre-treatment step causes slight roughening of NCT type I due to partial removal of the embedding a-C matrix. These changes have apparently no effect on the NP morphology.

## Discussion

In the following section the conclusions from the presented results for CVD growth of SWCNTs using C : Ni NCTs with and without predefined NPs are discussed.

### (a) NP stability of NCT type I.

Without stabilization, Ni thin films on  $\text{SiO}_2$  surfaces undergo clustering *via* surface diffusion for temperatures larger than  $-173$  °C.<sup>70,71</sup> Ni cluster diameters of 8 nm to 20 nm were reported for nominally 1 nm thick Ni films.<sup>71,72</sup> Bulk diffusion of Ni into a  $\text{SiO}_2$  layer on Si and formation of  $\text{NiSi}_2$  starts at elevated temperatures ( $\geq 425$  °C), depending on  $\text{SiO}_2$  thickness. The bulk diffusion onset temperature for a 2.5 nm thick  $\text{SiO}_2$  layer was reported to be 800 °C.<sup>70</sup> These data demonstrate that without stabilization much larger Ni particles are formed at temperatures similar to those during catalyst pre-treatment and CVD growth in the present study.

In fact, our investigations have shown that a defined microstructure of Ni-rich NPs with narrow diameter distribution of  $(2.0 \pm 0.3)$  nm can be stabilized up to temperatures of 735 °C and used to grow SWCNTs. This has been achieved by embedding the NPs in a protective matrix of a-C, forming a NCT of type I. The protective a-C is fully stable in ambient conditions and allows easy handling of the NCTs in air. Thus, the a-C matrix ensures the safe transport of the templates and their transfer into the CVD oven. During the pre-treatment step at 550 °C in air, the a-C matrix is partially conserved. This ensures that the Ni-rich NPs keep their initial positions, diameter distribution and spacing. In this way the NPs are prevented from coagulation and grain coarsening. This observation is attributed to the strong interaction between Ni and C, which is *e.g.* larger than that between Ni and  $\text{SiO}_2$ .<sup>73</sup> The rest of the a-C matrix presumably undergoes oxidation to  $\text{CO}_2$ . After pre-treatment, the NCT type I enters the CVD synthesis with pre-defined, almost unchanged diameter in activated form.

### (b) Relation between SWCNT and catalyst properties.

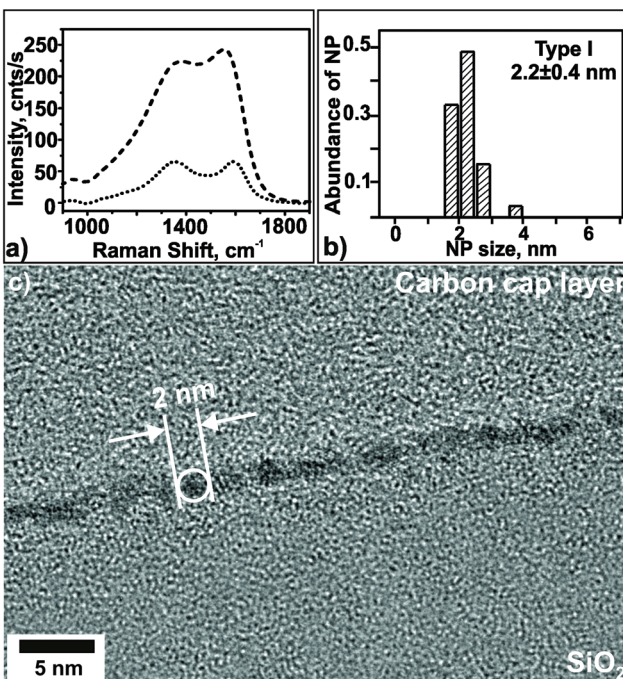


Fig. 7 Characterization of NCT type I after the pre-treatment step: (a) Raman spectrum (dotted line) in comparison to that of the pristine template (dashed line), (b) normalized size distribution of Ni-rich NPs measured by TEM, (c) cross-sectional TEM image.



It is obvious to explain the narrower and apparently selective SWCNT diameter distribution obtained by CVD growth using NCT type I by the pre-defined NP diameters and their demonstrated stability. As a consequence, the carbon precursors are exposed to almost equally-sized catalytically active NPs during the CVD process. In contrast to that situation, the initially homogeneously distributed Ni in NCT type II undergoes a coarsening, the carbon precursor is exposed to catalytic particles of different size and as a consequence, the SWCNT distribution is broader and not selective. On the other hand the smaller SWCNT diameters obtained with NCT type II can be attributed to the fact that NPs grow from an initially homogenous Ni distribution to a size of  $(2.5 \pm 0.8)$  nm. The behavior of NCT type II resembles catalysts whose catalytically active particles are formed *in situ* from metal thin films during the CVD process. The results presented here demonstrate that narrower SWCNT diameter distributions are accessible by the use of pre-defined, stable catalyst templates.

Apparently the best strategy to obtain SWCNTs with narrow diameter distribution is to use a catalyst with stable NPs of pre-defined size and to prevent them from coarsening during the CVD process. Several approaches to realize these preconditions were described in the literature. First, the catalyst NPs can be sparsely distributed over the inert substrate so that the large distance between the particles would prevent their aggregation.<sup>21,23,44,53</sup> For instance, Paillet *et al.*<sup>53</sup> studied the CVD synthesis of SWCNTs on Ni NPs with the mean size of  $(4.7 \pm 1.4)$  nm using  $\text{C}_2\text{H}_4$  as a carbon source. The narrow size distribution of SWCNTs was achieved at  $850^\circ\text{C}$  when the density of NPs and the synthesized SWCNTs was small (40 and 100 NPs per  $\mu\text{m}^2$  led to 0.1–0.2 and  $\sim 3$  SWCNTs per  $\mu\text{m}^2$ , respectively). Importantly, for these conditions the Ni NPs had the same size before and after the CVD. An increase of the surface density to several hundred NPs per  $\mu\text{m}^2$  led to aggregation of NPs and formation of amorphous carbon and big filamentous structures. An increase of the reaction temperature to  $950^\circ\text{C}$  also resulted in larger Ni NPs with broader size distribution.<sup>53</sup> In our work, a narrow SWCNT diameter distribution was successfully obtained with a much higher density of catalyst NPs (*ca.* 20 000 NPs per  $\mu\text{m}^2$ ) and synthesized SWCNTs (5–7 SWCNTs per  $\mu\text{m}^2$ ).

So far, the most successful approach to obtain SWCNTs with a narrow diameter distribution is the use of an inert matrix, which protects NPs from coarsening or makes this process much slower than SWCNT nucleation. Well-defined Fe NPs were obtained *in situ* by a preliminary process step and stabilized during CVD by embedding them in an aluminum oxide matrix.<sup>16,27,29,31</sup> This method offers catalyst NPs of different size with narrow diameter distribution on the substrate surface, but the size of NPs is not constant over the reaction time. The other widely used supports for nano-scaled metal catalysts are porous materials like mesostructured silica,<sup>32,33,36,39,40,45,74,75</sup> porous magnesium oxide<sup>24,34,47</sup> and zeolites,<sup>42,56,76</sup> which offer SWCNTs with a selective chirality<sup>32–34,36,39,45,74</sup> and sufficient yield. Catalyst particles immobilized in the substrate pores retain their size over reac-

tion time in a broad temperature range, however SWCNTs are formed not only on the surface but also in the bulk of the catalyst/matrix composite. As a result, they are bundled and inevitably mixed with the catalyst, which requires the use of laborious purification procedures.

In this work a new type of catalyst for diameter-selective SWCNT growth is presented. C:Ni nanocomposite template type I combines the following advantages: narrow catalyst diameter distribution, stability during the CVD process, potential for growing individual SWCNT with a significant length and yield. The study confirms the hypothesis that the diameter distribution of CVD-grown SWCNTs is determined by the catalyst morphology and the size of the catalyst particles at the initial point of the SWCNT nucleation.<sup>44,77</sup> In NCT type II, formation and growth of the catalyst NPs competes with the simultaneous SWCNT growth. Thus, the size distribution of the catalyst NPs is changing with time, and so does the diameter distribution of the nucleating SWCNTs. On the contrary, in NCT type I the catalyst NPs with narrow and weakly varying size distribution are available from the very beginning and during the whole time of the SWCNT growth. Hence, the diameter distribution of the synthesized SWCNTs is much narrower. Certainly, the study also shows that control of catalyst diameter is a necessary but not a sufficient condition for diameter-selective or even chirality-selective growth of SWCNTs. Further well-established parameters controlling the SWCNT diameter distribution are growth temperature, nature and concentration of precursors, and catalyst pre-treatment.

A final question that shall be briefly addressed is the chemical state of the catalytically active Ni-rich NPs. After the CVD process, fcc-Ni and  $\text{Ni}_3\text{C}$  were identified by the TEM analysis (Fig. 3 and ESI†). It is reasonable to assume that these two Ni phases are catalytically active. Fcc-Ni is commonly considered as most suitable Ni based catalyst for CNT growth.<sup>15,17,49,78</sup> Recent papers also reported  $\text{Ni}_3\text{C}$  as an active catalyst, at least for carbon nanofibers<sup>64</sup> and initial graphene layers of CNTs.<sup>50</sup> Moreover, indications for a minor fraction of  $\text{NiO}$  after the CVD process were obtained. A conclusion about its catalytic activity can however not be drawn on the basis of the presented results. *In situ* XPS and TEM studies could help to clarify the phase and chemical state of the catalytically active Ni species.

## Conclusions

A new type of pre-defined stable catalyst for diameter-controlled growth of SWCNTs was prepared and comprehensively characterized. It comprises dispersed catalytic particles, whose size is largely preserved during the CVD synthesis. This way, the problem of the Ostwald ripening is circumvented, and a new route for much better control over the diameter of CVD-grown SWCNTs is opened. Diameter-selectivity of NCT based SWCNT growth was demonstrated for the first time. A fraction of 50% of SWCNT diameters was confined to a range of  $(1.36 \pm 0.10)$  nm. In comparison to the growth using the pre-defined



NPs, a non-selective SWCNT distribution, with 88% of all SWCNT in the diameter range of 0.80 nm to 1.40 nm was obtained using a NCT with a homogenous microstructure under otherwise identical conditions (NCT type II).

The as-grown SWCNTs themselves are ideal candidates for further comprehensive characterization, *e.g.* by coupling of Raman spectroscopy with atomic force or scanning tunneling microscopy. They consist predominantly of separated SWCNTs, are free of solvents or surfactants, exhibit a low degree of bundling, and contain negligible amounts of MWCNTs. Their length to diameter ratio was of the order of 200. The narrow RBM line widths of 4 cm<sup>-1</sup> to 8 cm<sup>-1</sup> show a high structural order of the as-grown SWCNTs and point to a low amount of intrinsic structural defects and negligible nanotube bundle formation.

The presented approach opens a new way to perform CVD synthesis of SWCNTs using catalyst particles with well-defined size distribution. Usually in CVD growth of SWCNTs, the metallic NPs are synthesized *in situ*, which severely limits the possibility to reliably ascertain their homogeneity and quality. The NCTs used in this study can be prepared prior to CNT synthesis, are not destroyed when exposed to air, and their properties can be characterized with a high degree of certainty as described above.

Further optimization of the size distribution, stability, and catalytic activity of metallic NPs in NCTs promises even better control over the size and diameter distribution of CVD-synthesized SWCNTs. The a-C matrix could be replaced by thermally stable oxides, which would improve the stability of the catalytic NPs during CVD growth of SWCNTs. Moreover, the catalytic activity and diameter selectivity can be improved by using nanocomposite templates with embedded NP alloys like FeNi or FeCo instead of pure metals.

## Funding sources

This work was funded by the EU, “European Regional Development Fund”, Project ECEMP-D1 (no. 13857/2379), “Nanoskalige Funktionsschichten auf Kohlenstoffbasis”, and LEI 100114022 “C-basierte Funktionsschichten für tribologische Anwendungen”.

## Acknowledgements

Support by the Structural Characterization Facilities Dresden-Rossendorf at IBC is gratefully acknowledged. S.M. and S.G. acknowledge support of the Center of Advancing Electronics Dresden (CfAED). M.H. and M.K. thank NanoTP COST action for support. Additionally M.H. would like to acknowledge the operation team at the Binnig and Rohrer Nanotechnology Center for their support. Special thank by the authors is addressed to M. Missbach, A. Kunz, E. Christalle, A. Schneider, J. Wagner, B. Schreiber, L. Bischoff (all from HZDR) and T. Bayrak (Bilkent University Ankara) for technical

assistance, and K.-H. Heinig, R. Wenisch, D. Janke, A. Erbe (all from HZDR), and A. Popov (IFW Dresden) for helpful discussions and careful proofreading of the manuscript.

## Notes and references

- 1 S. Iijima, *Nature*, 1991, **354**, 56.
- 2 A. Bachtold, P. Hadley, T. Nakanishi and C. Dekker, *Science*, 2001, **294**, 1317.
- 3 W. J. Yu and Y. H. Lee, *ChemSusChem*, 2011, **4**, 890.
- 4 B. Liu, C. Wang, J. Liu, Y. Che and C. Zhou, *Nanoscale*, 2013, **5**, 9483.
- 5 P. Wick, M. J. D. Clift, M. Rösslein and B. Rothen-Rutishauser, *ChemSusChem*, 2011, **4**, 905.
- 6 Z. Liu, W. Cai, L. He, N. Nakayama, K. Chen, X. Sun, X. Chen and H. Dai, *Nat. Nanotechnol.*, 2007, **2**, 47.
- 7 K. Besteman, J.-O. Lee, F. G. M. Wiertz, H. A. Heering and C. Dekker, *Nano Lett.*, 2003, **3**, 727.
- 8 K. Bradley, A. Davis, J.-C. P. Gabriel and G. Grüner, *Nano Lett.*, 2005, **5**, 841.
- 9 M. F. L. De Volder, S. H. Tawfick, R. H. Baughman and A. J. Hart, *Science*, 2013, **339**, 535.
- 10 A. M. Ionescu and H. Riel, *Nature*, 2011, **479**, 329.
- 11 R. Saito, M. Fujita, G. Dresselhaus and M. S. Dresselhaus, *Appl. Phys. Lett.*, 1992, **60**, 2204.
- 12 T. W. Odom, J.-L. Huang, P. Kim and C. M. Lieber, *Nature*, 1998, **391**, 62.
- 13 J.-P. Tessonniere and D. S. Su, *ChemSusChem*, 2011, **4**, 824.
- 14 J. Prasek, J. Drbohlavova, J. Chomoucka, J. Hubalek, O. Jasek, V. Adam and R. Kizek, *J. Mater. Chem.*, 2011, **21**, 15872.
- 15 C. Journet, M. Picher and V. Jourdain, *Nanotechnology*, 2012, **23**, 142001.
- 16 W. Song, C. Jeon, Y. S. Kim, Y. T. Kwon, D. S. Jung, S. W. Jang, W. C. Choi, J. S. Park, R. Saito and C.-Y. Park, *ACS Nano*, 2010, **4**, 1012.
- 17 S. Hofmann, R. Sharma, C. Ducati, G. Du, C. Mattevi, C. Cepek, M. Cantoro, S. Pisana, A. Parvez, F. Cervantes-Sodi, A. C. Ferrari, R. Dunin-Borkowski, S. Lizzit, L. Petaccia, A. Goldoni and J. Robertson, *Nano Lett.*, 2007, **7**, 602.
- 18 R. Rao, D. Liptak, T. Cherukuri, B. I. Yakobson and B. Maruyama, *Nat. Mater.*, 2012, **11**, 213.
- 19 A. R. Harutyunyan, G. Chen, T. M. Paronyan, E. M. Pigos, O. A. Kuznetsov, K. Hewaparakrama, S. M. Kim, D. Zakharov, E. A. Stach and G. U. Sumanasekera, *Science*, 2009, **326**, 116.
- 20 P. Petit, D. Salem, M. He, M. Paillet, R. Parret, J.-L. Sauvajol and A. Zahab, *J. Phys. Chem. C*, 2012, **116**, 24123.
- 21 L. Durrer, J. Greenwald, T. Helbling, M. Muoth, R. Riek and C. Hierold, *Nanotechnology*, 2009, **20**, 355601.
- 22 B. Zhao, D. N. Futaba, S. Yasuda, M. Akoshima, T. Yamada and K. Hata, *ACS Nano*, 2009, **3**, 108.
- 23 D. Takagi, Y. Homma, H. Hibino, S. Suzuki and Y. Kobayashi, *Nano Lett.*, 2006, **6**, 2642.



24 I. Abdullahi, N. Sakulchaicharoen and J. E. Herrera, *Diamond Relat. Mater.*, 2014, **41**, 84.

25 H. Ago, T. Ayagaki, Y. Ogawa and M. Tsuji, *J. Phys. Chem. C*, 2011, **115**, 13247.

26 C. L. Cheung, A. Kurtz, H. Park and C. M. Lieber, *J. Phys. Chem. B*, 2002, **106**, 2429.

27 S. Sakurai, M. Inaguma, D. N. Futaba, M. Yumura and K. Hata, *Small*, 2013, **9**, 3584.

28 H. Liu, D. Takagi, S. Chiashi and Y. Homma, *Nanotechnology*, 2009, **20**, 345604.

29 M. Cantoro, S. Hofmann, S. Pisana, V. Scardaci, A. Parvez, C. Ducati, A. C. Ferrari, A. M. Blackburn, K. Y. Wang and J. Robertson, *Nano Lett.*, 2006, **6**, 1107.

30 E. Suvaci, Y. Çelik, A. Weibel, A. Peigney and E. Flahaut, *Carbon*, 2012, **50**, 3092.

31 S. M. Kim, C. L. Pint, P. B. Amama, D. N. Zakharov, R. H. Hauge, B. Maruyama and E. A. Stach, *J. Phys. Chem. Lett.*, 2010, **1**, 918.

32 H. Wang, L. Wei, F. Ren, Q. Wang, L. D. Pfefferle, G. L. Haller and Y. Chen, *ACS Nano*, 2013, **7**, 614.

33 S. M. Bachilo, L. Balzano, J. E. Herrera, F. Pompeo, D. E. Resasco and R. B. Weisman, *J. Am. Chem. Soc.*, 2003, **125**, 11186.

34 M. He, H. Jiang, B. Liu, P. V. Fedotov, A. I. Chernov, E. D. Obraztsova, F. Cavalca, J. B. Wagner, T. W. Hansen, I. V. Anoshkin, E. A. Obraztsova, A. V. Belkin, E. Sairanen, A. G. Nasibulin, J. Lehtonen and E. I. Kauppinen, *Sci. Rep.*, 2013, **3**, 1460.

35 M. He, A. I. Chernov, P. V. Fedotov, E. D. Obraztsova, E. Rikkinen, Z. Zhu, J. Sainio, H. Jiang, A. G. Nasibulin, E. I. Kauppinen, M. Niemela and A. O. Krause, *Chem. Commun.*, 2011, **47**, 1219.

36 N. Li, X. Wang, F. Ren, G. L. Haller and L. D. Pfefferle, *J. Phys. Chem. C*, 2009, **113**, 10070.

37 M. Fouquet, B. C. Bayer, S. Esconjauregui, R. Blume, J. H. Warner, S. Hofmann, R. Schlögl, C. Thomsen and J. Robertson, *Phys. Rev. B: Condens. Matter*, 2012, **85**, 235411.

38 B. Liu, W. Ren, S. Li, C. Liu and H.-M. Cheng, *Chem. Commun.*, 2012, **48**, 2409.

39 L. Wei, S. Bai, W. Peng, Y. Yuan, R. Si, K. Goh, R. Jiang and Y. Chen, *Carbon*, 2014, **66**, 134.

40 H. Wang, K. Goh, R. Xue, D. Yu, W. Jiang, R. Lau and Y. Chen, *Chem. Commun.*, 2013, **49**, 2031.

41 S. Noda, Y. Tsuji, Y. Murakami and S. Maruyama, *Appl. Phys. Lett.*, 2005, **86**, 173106.

42 S. Maruyama, R. Kojima, Y. Miyauchi, S. Chiashi and M. Kohno, *Chem. Phys. Lett.*, 2002, **360**, 229.

43 K. Kakehi, S. Noda, S. Maruyama and Y. Yamaguchi, *Appl. Surf. Sci.*, 2008, **254**, 6710.

44 M. Fouquet, B. C. Bayer, S. Esconjauregui, C. Thomsen, S. Hofmann and J. Robertson, *J. Phys. Chem. C*, 2014, **118**, 5773.

45 H. Wang, B. Wang, X.-Y. Quek, L. Wei, J. Zhao, L.-J. Li, M. B. Chan-Park, Y. Yang and Y. Chen, *J. Am. Chem. Soc.*, 2010, **132**, 16747.

46 M. Picher, E. Anglaret, R. Arenal and V. Jourdain, *ACS Nano*, 2011, **5**, 2118.

47 H. J. Jeong, K. H. An, S. C. Lim, M.-S. Park, J.-S. Chang, S.-E. Park, S. J. Eum, C. W. Yang, C.-Y. Park and Y. H. Lee, *Chem. Phys. Lett.*, 2003, **380**, 263.

48 M. Krause, M. Haluška, G. Abrasonis and S. Gemming, *Phys. Status Solidi B*, 2012, **249**, 2357.

49 A. Achour, A. A. El Mel, N. Bouts, E. Gautron, E. Grigore, B. Angleraud, L. Le Brizoual, P. Y. Tessier and M. A. Djouadi, *Diamond Relat. Mater.*, 2013, **34**, 76.

50 N. T. Panagiotopoulos, E. K. Diamanti, L. E. Koutsokeras, M. Baikousi, E. Kordatos, T. E. Matikas, D. Gournis and P. Patsalas, *ACS Nano*, 2012, **6**, 10475.

51 H. Ago, Y. Nakamura, Y. Ogawa and M. Tsuji, *Carbon*, 2011, **49**, 176.

52 K. Kakehi, S. Noda, S. Chiashi and S. Maruyama, *Chem. Phys. Lett.*, 2006, **428**, 381.

53 M. Paillet, V. Jourdain, P. Poncharal, J.-L. Sauvajol, A. Zahab, J. C. Meyer, S. Roth, N. Cordente, C. Amiens and B. Chaudret, *J. Phys. Chem. B*, 2004, **108**, 17112.

54 W.-H. Chiang and R. Mohan Sankaran, *Nat. Mater.*, 2009, **8**, 882.

55 H. Sugime, S. Noda, S. Maruyama and Y. Yamaguchi, *Carbon*, 2009, **47**, 234.

56 Y. Miyauchi, S. Chiashi, Y. Murakami, Y. Hayashida and S. Maruyama, *Chem. Phys. Lett.*, 2004, **387**, 198.

57 G. Abrasonis, M. Krause, A. Mücklich, K. Sedláčková, G. Radnóci, U. Kreissig, A. Kolitsch and W. Möller, *Carbon*, 2007, **45**, 2995.

58 M. Krause, A. Mücklich, T. W. H. Oates, M. Zschornak, S. Wintz, J. Luis Endrino, C. Baehtz, A. Shalimov, S. Gemming and G. Abrasonis, *Appl. Phys. Lett.*, 2012, **101**, 053112.

59 M. Krause, M. Buljan, A. Mücklich, W. Möller, M. Fritzsche, S. Facska, R. Heller, M. Zschornak, S. Wintz, J. L. Endrino, C. Baehtz, A. Shalimov, S. Gemming and G. Abrasonis, *Phys. Rev. B: Condens. Matter*, 2014, **89**, 085418.

60 S. Reich, C. Thomsen and J. Maultzsch, *Carbon nanotubes: basic concepts and physical properties*, Wiley-vch, 2004.

61 International center for diffraction data, vol. card 00-004-0850 for fcc Ni, card 01-089-7129 for hexagonal Ni, card 04-007-3753 for rhombohedral nickel carbide, card 01-078-0429 for fcc NiO.

62 G. Abrasonis, A. C. Scheinost, S. Zhou, R. Torres, R. Gago, I. Jiménez, K. Kuepper, K. Potzger, M. Krause, A. Kolitsch, W. Möller, S. Bartkowski, M. Neumann and R. R. Gareev, *J. Phys. Chem. C*, 2008, **112**, 12628.

63 S. Uhlig, R. Struis, H. Schmid-Engel, J. Bock, A.-C. Probst, O. Freitag-Weber, I. Zizak, R. Chernikov and G. Schultes, *Diamond Relat. Mater.*, 2013, **34**, 25.

64 B. W. Yu, Q. K. Zhang, L. Z. Hou, S. L. Wang, M. Song, Y. H. He, H. Huang and J. Zou, *Carbon*, 2016, **96**, 904.

65 D. B. Williams and C. B. Carter, in *Transmission Electron Microscopy: A Textbook for Materials Science*, Springer, US,



Boston, MA, 2009, p. 283, DOI: 10.1007/978-0-387-76501-3\_18.

66 A. Jorio, A. G. Souza, G. Dresselhaus, M. S. Dresselhaus, A. K. Swan, M. S. Unlu, B. B. Goldberg, M. A. Pimenta, J. H. Hafner, C. M. Lieber and R. Saito, *Phys. Rev. B: Condens. Matter*, 2002, **65**, 155142.

67 R. Pfeiffer, H. Kuzmany, C. Kramberger, C. Schaman, T. Pichler, H. Kataura, Y. Achiba, J. Kurti and V. Zolyomi, *Phys. Rev. Lett.*, 2003, **90**, 225501.

68 P. T. Araujo, S. K. Doorn, S. Kilina, S. Tretiak, E. Einarsson, S. Maruyama, H. Chacham, M. A. Pimenta and A. Jorio, *Phys. Rev. Lett.*, 2007, **98**, 067401.

69 J. Maultzsch, H. Telg, S. Reich and C. Thomsen, *Phys. Rev. B: Condens. Matter*, 2005, **72**, 205438.

70 J. T. Mayer, R. F. Lin and E. Garfunkel, *Surf. Sci.*, 1992, **265**, 102.

71 P. H. Lee and C. C. Chang, *Surf. Sci.*, 2007, **601**, 362.

72 J. B. Zhou, T. Gustafsson, R. F. Lin and E. Garfunkel, *Surf. Sci.*, 1993, **284**, 67.

73 M. Aral, T. Ishikawa and Y. Nishiyama, *J. Phys. Chem.*, 1982, **86**, 577.

74 A. Jorio, A. P. Santos, H. B. Ribeiro, C. Fantini, M. Souza, J. P. M. Vieira, C. A. Furtado, J. Jiang, R. Saito, L. Balzano, D. E. Resasco and M. A. Pimenta, *Phys. Rev. B: Condens. Matter*, 2005, **72**, 075207.

75 C. Zoican Loebick, R. Podila, J. Reppert, J. Chudow, F. Ren, G. L. Haller, A. M. Rao and L. D. Pfefferle, *J. Am. Chem. Soc.*, 2010, **132**, 11125.

76 T. Moteki, D. Nukaga, Y. Murakami, S. Maruyama and T. Okubo, *J. Phys. Chem. C*, 2014, **118**, 23664.

77 R. Sharma, P. Rez, M. M. J. Treacy and S. J. Stuart, *J. Electron Microsc.*, 2005, **54**, 231.

78 M. H. Kuang, Z. L. Wang, X. D. Bai, J. D. Guo and E. G. Wang, *Appl. Phys. Lett.*, 2000, **76**, 1255.

